Solutions for eclipsing binaries of bulge field in OGLE II using the Detached Eclipsing Binary Light curve fitter (DEBiL)

Jonathan Devor[1]

Abstract

We present solutions and analysis of 10862 detached and semi-detached eclipsing binary systems in the bulge fields of OGLE II, obtained by using a new method for light curve fitting[2]. This new method, the Detached Eclipsing Binary Light curve fitter (DEBiL) has as its primary design goals: speed and full automation. Its speed is due to the employment of a simple binary system model, efficient algorithm and parallelizability. Both its speed and its elimination of the need for human guidance make it practical to analyze today's largest light curve datasets, as well as the still larger ones that will be available in the future.

1. Introduction

Eclipsing binary star systems provide one of the only direct methods for measuring the mass and radii of stars outside the solar neighborhood, which is needed for better understanding the stellar physics of these stars. It is especially important to make these measurements for low mass main sequence stars (i.e. M-dwarfs and smaller), since only three binaries of such stars are currently known. Some important consequences of locating more such binary systems, include more accurate calibration of the local distance latter [Local group: Paczynski 1997, M31: Kaluzny 1997], constraining the low mass IMF and discovering extrasolar planets, in the limiting case where one of the two binary components has zero brightness.

In order to determine all of the orbital parameters of the binary systems, both eclipsing and radial velocity data are needed. While all eclipsing systems can have measurable radial velocities, only a small fraction of systems with known radial velocities eclipse. This asymmetry is because as long as the binary system orbit is not perfectly face-on, it will have some amount of radial velocity, while eclipses will only occur in systems that are almost edge on. A binary system with a circular orbit, with combined semi-major axis (a) and stellar radii (r_1, r_2), will eclipse when its inclination angle (i) meets the following criterion:

[1] The Harvard-Smithsonian Center for Astrophysics, 60 Garden Street, Cambridge, MA 02138 ; jdevor@cfa.harvard.edu

[2] The list of OGLE II bulge field model solutions as well as the latest version of the DEBiL source code are available online.

$$\cos(i) < \frac{r_1 + r_2}{a} \tag{1}$$

Assuming that the inclination angle (i) is randomly distributed, this condition becomes increasingly restrictive with a probability of:

$$p_{eclipse} = \frac{2}{\pi} \cdot \arcsin\left(\frac{r_1 + r_2}{a}\right) \approx \frac{2}{\pi} \cdot \frac{r_1 + r_2}{a} \tag{2a}$$

$$p_{eclipse} = \frac{r_1 + r_2}{a} \tag{2b}$$

Where (eq. 2a) is assuming a uniform distribution and (eq. 2b) is assuming a more realistic $p(i)di \propto |\sin(i)|di$ distribution.

The only way to compensate for these low probabilities is by observing increasingly large numbers of variable star systems, as we become interested in more detached systems with smaller probabilities for eclipsing.

During the past decade there have been many light curve surveys [e.g. OGLE: Udalski 1994 ; EROS: Beaulieu 1995 ; DUO: Alard 1997 ; MACHO: Alcock 1998] that take advantage of technical advances in robotic telescopes [Genet 1989 ; Hall 1995] and photometric analysis, such as difference image analysis (DIA) [Crotts 1992 ; Phillips 1995]. The original goal of most of these surveys was not the search for eclipsing binaries, but rather to search for gravitational microlensing events [Paczynski 1986]. Fortunately, the data derived from these surveys are ideal for eclipsing binary searches as well. In this paper, we will present results obtained by analyzing data from the second phase of the Optical Gravitational Lensing Experiment (OGLE II) in the galactic bulge field [Udalski 1997 ; Mizerski 2002 ; Wozniak 2002], though the same analysis could have been performed on any light curve dataset. The underlying motivation for this project was to provide a method for taking advantage of the impending deluge of data derived from the growing observational and computational capabilities of automated surveys and from the fact that a growing fraction of the existing data are becoming publicly available [Szalay 2001].

Fitters for eclipsing binary models are generally based on accurate yet complex models [Wilson 1971 ; Nelson 1972 ; Wilson 1979 ; Etzel 1981 ; Claret 2003b] that require substantial human intervention (e.g. for identifying outliers and guiding the numerical convergence). The need for human involvement brings about an inherent bottleneck to the pipeline, which prevents it from being able to handle the expected quantities of future data. Even attempts to automate the convergence process (e.g. [Wyithe 2001]), still rely on a-priori knowledge of the systems for setting the initial starting point of the convergence. This type of human decision-making adds, by definition, an element of subjectivity and thus inconsistency in the final results. In this project, we have used a simple model, with a minimal number of free parameters and have made the pipeline entirely automated, with no a-priori assumptions outside of the model itself. This strict requirement could be construed as a handicap, however biases that may result from the automated process are likely to be far more consistent and ultimately correctable than the biases of alternative approaches. In addition, by employing a simplified model, it is

possible to fit a model more rapidly, enabling both the timely analysis of larger datasets and a more nimble convergence method that is comprised of many thousands of small steps, instead of a few dozen large ones. Finally, by making the pipeline easily parallelizable, with minimal memory requirements of each processor (currently less than 1 megabyte) and no inter-processor communication, it can be easily scaled to an arbitrary size. Once the entire given data set has been fit to first order, more refined fittings can be performed on a smaller number of selected light curves.

2. Method

2.1. Overview of the pipeline

This project was designed around the analysis of eclipsing binary star systems within the OGLE II (bulge field) dataset of light curves. Though the pipeline is designed to process any group of light curves, there are a number of settings in the implementation that are optimized for this dataset and for currently available computers. These settings will be noted in the following description of the pipeline implementation.

The pipeline for this project consists of three fundamental stages. For each given light curve, one needs to first find its period, then "guess" its model parameters and finally numerically refine the model parameters. At present, a typical timescale for running these steps is on the order of 10 minutes, where almost all the computing time is split between the first and third stage. As we will see in the following subsections, this time can be reduced, but at the expense of the accuracy of the derived result. In order that hundreds of thousands or even millions of light curves may be processed accurately, in a reasonable amount of time, we need to both add filtering steps to the pipeline and parallelize it. Fortunately, because each light curve is completely independent of the others, parallelizing the pipeline is very easy. One simply must divide the given group of light curves into subgroups[3], run each subgroup on a different CPU and import the results into a single database. It is with the filtration steps were one needs to be most cautious

The optimal method of filtration is to filter out all the undesirable light curves after each stage. In other words, each stage in the pipeline is split into two steps: a processing step and a filtering step. The resulting pipeline has the following six steps:

1) Find the period
2) Filter out non-periodic light curves
3) Find an "initial guess" for the eclipsing binary model parameters
4) Filter out non-eclipsing binaries (at least semi-detached)
5) Numerically fit the parameters in eclipsing binary model
6) Filter out unsuccessful fits

[3] Ideally, the size of each of these subgroups will be proportional to the effective speed of the computer they are being run on.

Step (1) can be performed using any "off-the-shelf" periodogram algorithm. In our implementation, we scanned periods starting from a tenth of a day and selected the period that minimizes the variance around a second order fit in each of eight phase bins. The variances of the eight bins were combined to make a single score, using the analysis of variances (AOV) algorithm [Schwarzenberg-Czerny 1989, Schwarzenberg-Czerny 1996]. In the case of our dataset, there were strong periodogram spikes at a period of a sidereal day and its rational multiples due to the sampling window function (with diminishing power with the size of the numerator and denominator). For this reason periods around a sidereal day and the 12 subsequent most power rational multiples were suppressed. Fortunately, due to the algorithm employed, these problematic period ranges were quite small. Assuming that the period likelihood curve is smooth, we expect that less than 1% of the periodic variables fall within these problematic period ranges. Finally, once the period has been located and finely tuned, rational multiples, with a numerator and denominator from 1 to 19 are checked. A more complete description and analysis of this method will be given in a forthcoming paper.

Step (2) requires a threshold for filtering out all but the variables with a strong periodic component. The threshold chosen was of a periodic strength score of 6.5 (vertical dashed line). Only light curves with this strength score or higher continued on to the following step. In addition to this, we set a requirement that the variables' period will be no more than 200 days, which guarantees at least four foldings. These criteria filtered out ~90% of all the light curves in the dataset. This cutoff was selected to be on the side of caution in order to minimize polluting the model fitter with non-binaries and very noisy data.

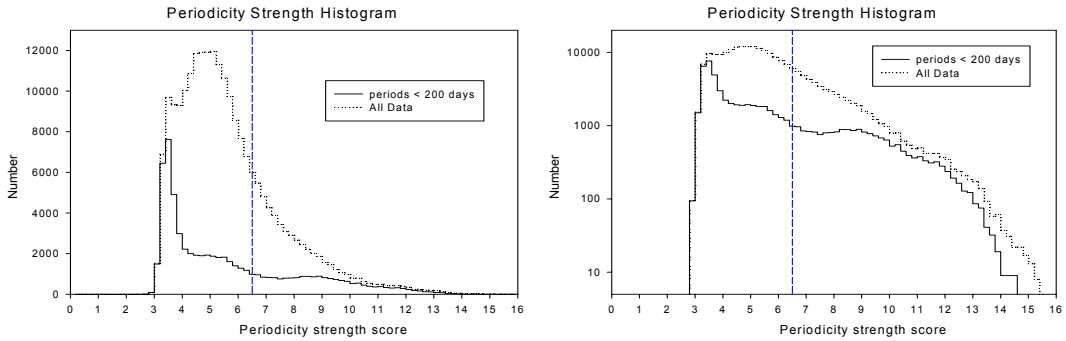

Figure 1. The distribution of periodicity strengths in the OGLE II (bulge field) dataset. Only light curves with both periodicity strength of at least 6.5 and periods less than 200 days were used in the subsequent pipeline steps.

Steps (3) through (5) are all performed within the DEBiL program. Step (3) is implemented by the "initial guess" equations described in detail in subsection 2.3. Step (4) verifies the results given by the "initial guess" equations. Step (5) simulates the light curves that would have been seen with the parameters found by the "initial guess" and systematically varies the parameters so to get the best fit to the data. The way these light curve simulation are rapidly created is described in subsection 2.4. The algorithm for

choosing which variances should be tested and how to converge the parameters is described in subsection 2.5.

Step 6 is the only non-generic part of the pipeline. Each DEBiL user should implement this step to fit the needs of his or her research requirements. DEBiL provides a number of auxiliary tests described in subsection 2.7 and in appendix B. These tests are designed to provide additional information on the quality of the fit. In our implementation we chose, based on appearance, a simple upper limit on the reduced χ^2 test: $\chi^2_\nu < 4$

The final result of our pipeline contained only about 5% of the total number of light curves we started with. The filtration process was as follows:

- Total number of OGLE II (bulge field) variables: 218699
- After step 2, with strong periodicity and periods of 0.1-200 days: 19265
- After step 4, the output of the DEBiL program: 17767
- After step 6, with good fits to binary models: 10862

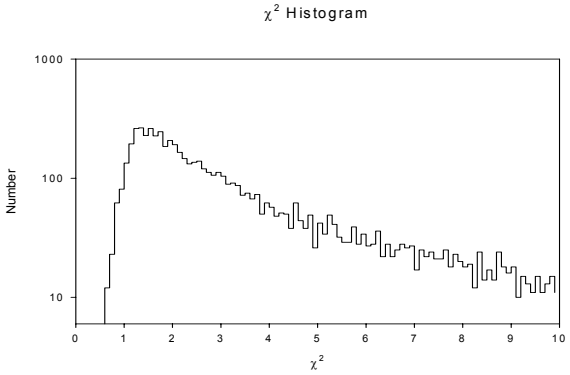

Figure 2. The distribution of χ^2_ν fits of the DEBiL fitter

Additional filtering is recommended in order to cull out non-binary light cures that either look a lot like binaries or have erroneously large error estimates. Both of these may produce low reduces chi square results. The price of these filtering is that even with careful cuts, it is virtually inevitable that proper binary light curves will be thrown out too (this is also a problem in step 6). In order to handle the large error estimates, we calculate a given model's chi score (see appendix B) and filter it out if it has a chi score smaller than 0.9. Handling non-binary light curve that look like binary light curves is much more problematic. A common such case is with pulsating stars, which can have a light curve that mimics an eclipsing binary. Fortunately their light typically has a sinusoidal shape. To this end, we filter out models with reduced chi square larger than the reduced chi square of a best-fit sinusoidal function (fitting the amplitude and DC component). To handle period doubling, we fit both a sinusoidal function with the phased period and a sinusoidal function with half the phased period. After both these filtrations we have 8471 remaining light curves.

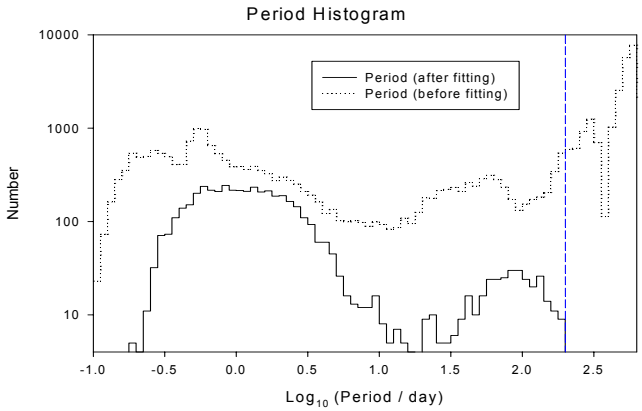

Figure 3. The distribution of periods. The dotted line represents all the strongly periodic light curves (periodicity strength > 6.5) and the solid line represents the light curves for which an acceptable model fit ($\chi^2_\nu < 4$) was found. The vertical dashed line marks the 200-day period threshold, beyond which light curves were no longer considered. Note that in addition to filtering out light curves, the DEBiL program also doubles the period for binaries with closely symmetric dips, which were mistakenly folded to half their correct period by the period-finder. Note the bimodal distribution above and below ~20 days. Also note that, though small by fraction, there are a notable number of binaries with periods less than half a day. Since DEBiL is only designed to handle detached binaries, these fits are presumably less accurate.

2.2 Model

For our model, we will consider a perfectly detached binary star system (i.e. perfectly spherical stars in elliptical orbits, with no tidal interaction, gravity darkening or reflections). In addition we will ignore any surface activity (e.g. spots and flares), which can be looked at from the model residuals. Finally, we will assume that there is no 3rd star blending. This last assumption may be the most problematic, but since this information is degenerate with the binary brightness, we must ignore it.

In this regime, classical 2-body Newtonian mechanic describes well the dynamics of the systems. There are 8 parameters that completely describe such 2-body orbits in three dimensions:

a_1, a_2 = Semi-major axes of the respective two bodies
e = Eccentricity of the orbit
i = Orbital inclination (i.e. the angle between orbital normal and the line of sight)
Ω = Longitude of ascending node
ω = Argument of perihelion
t_0 = Epoch of perihelion
P = the period of the orbit

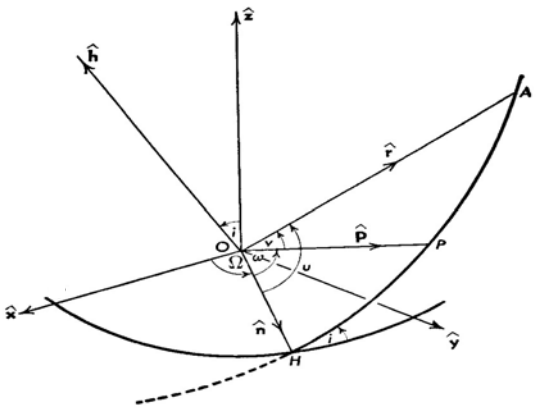

Figure 4. Orbital motion in 3-dimentional space, where the $\hat{z}$ -axis is defined as the line of sight and the $\hat{x}, \hat{y}$ axes are arbitrary. Point H is the ascending node and point P is the pericenter. [Taken from Danby 1964]

Since we can't spatially resolve the individual stars of the binary, the longitude of the ascending node (Ω) becomes completely degenerate and we can only consider the sum of the semi-major axes: $a \equiv a_1 + a_2$

For mathematical convenience, we will set the units such that: P=1 and a=1 (which defines the time scale and the length scale). This leaves us with 4 independent parameters describing the binary orbit. In addition there are 4 dominant parameters describing the stars themselves:

r_1, r_2 = The respective star's radius

B_1, B_2 = The respective star's central surface brightness (flux per unit solid angle - using arbitrary units)

This brings the total number of free parameters back to 8.

A final effect that needs to be taken into account is the limb darkening of the binary stars. Here, we will use a quadratic approximation of limb darkening, as seen through a Johnson I-filter [Claret 1998a ; Claret 2003], used in the OGLE II survey, assuming constant solar-like characteristics with an effective surface temperature: $T_{eff} = 5800^{\circ} K$ and a surface gravitational acceleration (in CGS units): $Log_{10}(g) = 4.5$

Note that while the limb darkening effect itself is not negligible, in order to minimize the number of free parameters that must be fit, we are neglecting the variation of limb darkening from one star to another.

2.3 "Initial guess"

In this subsection, we will describe an analytic approximation for the eclipsing binary model parameters. It generalizes the analytic solution for circular orbits [Seager 2002]. This solution will be obtained by consecutively bootstrapping the parameters in five steps:

2.3.1 Finding the larger radius:

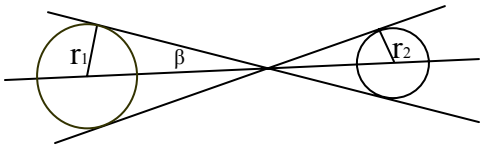

Figure 5: Two stars in an approximately circular orbit. Note that the line crossing is *not* the center of mass or the rotation pivot.

We will begin by approximating a circular orbit. From this, we find:

$$\frac{r_1 + r_2}{a} = \sin\beta \tag{3a}$$

$$\beta \approx \pi \cdot \frac{FWHM}{P} \tag{3b}$$

Combining these equations together, and assuming $r_1 >> r_2$

$$\frac{r_1}{a} \approx \sin\left(\pi \cdot \frac{FWHM}{P}\right) \tag{4}$$

Thus we can approximately find β from the full width at half the dip's minima. Despite this crude approximation, the derived results are remarkably accurate.

2.3.2 Finding the smaller radius and the central surface brightnesses:

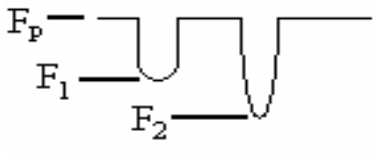

Figure 6: The general features of an eclipsing binary light curve

Once we have the value of the larger radius, we can find the value of the smaller radius, as well as the brightness of the two stars, using the following relatively easily measurable flux values:

F_p = Plateau flux

F_1 = Flux at the bottom of dip #1

F_2 = Flux at the bottom of dip #2

To avoid ambiguity between the two dips, we measure the time difference between their minima. If the difference is smaller than half the period, the first dip is labeled #1 and the second is labeled #2. Otherwise the first is #2 and the second is #1. This guarantees that the wrapped (modulo) time period from dip #1 till dip #2 is less than half the period. The physical consequence of this is that dip #1 is immediately before the epoch of perihelion and dip #2 is immediately after it.

There are two distinct possibilities that need to be checked: $r_1 > r_2$ and $r_1 < r_2$

We will limit our discuss to the former. In the latter case one simply needs to swap the 1 and 2 indexes.

Dip #1 (before perihelion) is created as the large star (r_1) eclipses the smaller star (r_2), this will often create a flat-bottomed dip. One shouldn't rely on the existence of a flat bottom in this case, since quite often eclipses are grazing. Dip #2 (after perihelion) is created when the small star partially eclipses the large star, which gives its light curve a rounded bottom as it passes in front of regions of the large star's disk, with varying of limb darkening.

B_1, B_2 = Respective central surface brightness

S_1, S_2 = Respective effective disk area (compensating for the limb darkening)

$$\begin{cases} F_p = (S_1 \cdot B_1) + (S_2 \cdot B_2) \\ F_1 = S_1 \cdot B_1 \\ F_2 \approx (S_1 \cdot B_1) + (S_2 \cdot B_2) - (B_1 \cdot S_2) \end{cases} \quad (5)$$

The third equation assumes a small limb darkening effect. For a more accurate calculation, one needs to know the projected impact parameter of the stars and integrate the flux of star 1 within the disk of star 2. An intermediate approach would be to assume a zero projected impact parameter and integrate limb darkening of star 1 from its center to r_2. Given r_1 (from 2.3.1), we can then bootstrap a solution for r_2, B_1, B_2 in the following manner:

$$
\begin{aligned}
&r_1 \to S_1 \\
&B_1 = \frac{F_1}{S_1} \\
&S_2 \approx \frac{F_p - F_2}{B_1} \to r_2 \\
&B_2 = \frac{F_p - F_1}{S_2}
\end{aligned}
\tag{6}
$$

2.3.3 Finding the eccentricity and the argument of perihelion:

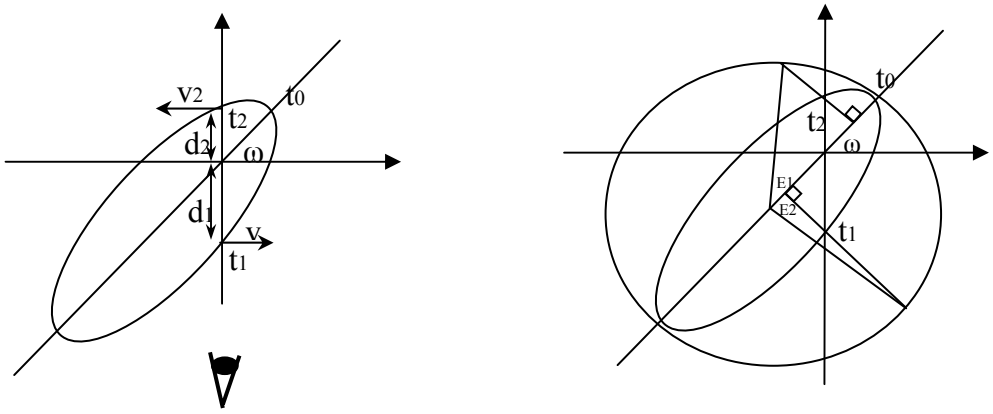

Figure 7: A diagram of the velocities (left) and mean anomolies (right) of one of the stars. The perihelion is at t_0 and the two eclipses occur at t_1 and t_2, so that $t_1 \le t_0 \le t_2$.

From the conservation of angular momentum, we have:

$$
d_1 \cdot v_1 = d_2 \cdot v_2 = \left(\vec{d} \times \vec{v}\right)_z = \frac{2\pi \cdot a^2 \cdot \sqrt{1-e^2}}{P} \tag{7}
$$

The radial distance of the stars is known from their elliptical orbit

$$
d_{1,2} = \frac{a\left(1-e^2\right)}{1 \mp e \sin\omega} \tag{8}
$$

Which allows us to solve for the tangential component of the velocities

$$
v_{1,2} = \frac{2\pi \cdot a \cdot \left(1 \mp e \sin\omega\right)}{P \cdot \sqrt{1-e^2}} \tag{9}
$$

Given the width of the dips ($W_{1,2}$):

$$W_{1,2} \propto \frac{1}{v_{1,2}} = \frac{P \cdot \sqrt{1-e^2}}{2\pi \cdot a \cdot (1 \mp e \sin\omega)} \tag{10}$$

Looking at the width ratio

$$\frac{W_1}{W_2} = \frac{1 + e\sin\omega}{1 - e\sin\omega} \tag{11}$$

This becomes

$$e\sin\omega = \frac{W_1 - W_2}{W_1 + W_2} \tag{12}$$

The mean anomalies at the two dips ($E_{1,2}$) can be shown to have an analytic solution (see fig. 7), presented below in two equivalent forms, with $-\pi \le \omega \le \pi$

$$E_{1,2} = \arcsin\left(\frac{\sqrt{1-e^2}\cos\omega}{e\sin\omega \mp 1}\right) \tag{13a}$$

$$E_{1,2} = \mp \arccos\left(\frac{e \mp \sin\omega}{1 \mp e\sin\omega}\right) \tag{13b}$$

Setting this solution into Kepler's equation

$$(t_{1,2} - t_0)\cdot\frac{2\pi}{P} = E_{1,2} - e\sin E_{1,2} \tag{14}$$

We can derive the time between the two eclipses (Δt)

$$2\pi\frac{\Delta t}{P} = \frac{2\pi}{P}(t_2 - t_1) = (E_2 - E_1) - e(\sin E_2 - \sin E_1) \tag{15}$$

This becomes

$$\pi\frac{\Delta t}{P} = \arccos\left(\frac{e\cos\omega}{\sqrt{1-e^2\sin^2\omega}}\right) - \frac{\sqrt{1-e^2}\cdot e\cos\omega}{1-e^2\sin^2\omega} \tag{16}$$

This enables us to find the value of: $(e\cos\omega)$, given $\frac{\Delta t}{P}$ and $(e\sin\omega)$, which gives us both the eccentricity of the system and its argument of perihelion. This equation must be solved numerically, but this is straight forward, since $\frac{\Delta t}{P}$ monotonically decreases with $(e\cos\omega)$.

2.3.4 Finding the epoch of perihelion:

We will now make a derivation similar to that of the pervious section, only now we *add* the two instances of Kepler's equation

$$\frac{-4\pi}{P}\left(t_0 - \frac{t_1 + t_2}{2}\right) = \left(E_2 + E_1\right) - e\left(\sin E_2 + \sin E_1\right) \tag{17}$$

Which becomes

$$\frac{2\pi}{P}\left(t_0 - \frac{t_1 + t_2}{2}\right) = sign(\omega)\cdot \arccos\left(\frac{\cos\omega}{\sqrt{1 - e^2 \sin^2(\omega)}}\right) - \frac{\sqrt{1-e^2}\cdot e^2 \sin\omega\cos\omega}{1 - e^2\sin^2\omega} \tag{18}$$

Together with the results of 2.3.3, the epoch of perihelion (t_0) can be readily solved.

2.3.5 Finding sin(i):

So far, we implicitly assumed sin(i)=1 for all the previous calculation, but this only effects the dip widths and calculation involving limb darkening and has little or no effect on the remaining parameters. This calculation is only a crude approximation, since we need to ignore the limb darkening and assume that one star is significantly larger than the other ($r_1 >> r_2$). Thus, the edge of the larger star will be approximately straight compared to the edge of the smaller star. In addition, assume here that the stars don't just graze each other, rather the smaller star, at some point, completely overlaps the larger star.

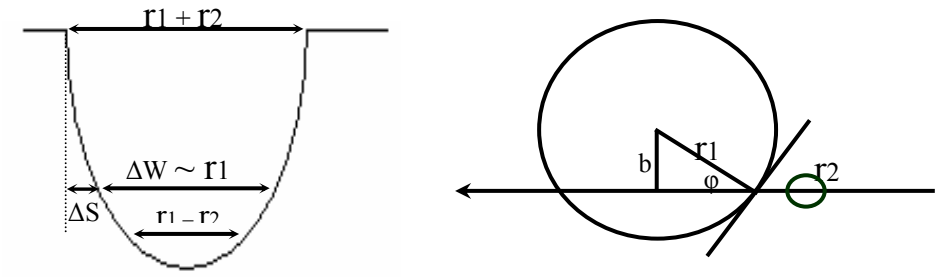

Figure 8: Diagrams of a light curve of an eclipse with zero impact parameter (left) and the relative tangential motion of the binary star system (right)

Using all these approximations, we can derive the following relations for the time interval during which the smaller star completely overlaps the larger one (ΔW) and the time interval of the partial overlap (ΔS). The former can be defined as the "flat-bottom" time interval and the latter as the "ingress/egress" time interval. Knowing when each of these intervals begins and ends in a given light curve is a non-trivial problem. In our

implementation we set ΔW as the full width at half minimum (FWHM), and ΔS as double the interval from three quarters minimum to a quarter minimum.

$$\begin{cases} \Delta W_{1,2} \approx \dfrac{2 \cdot \sqrt{r_1^2 - b^2}}{v_{1,2}} = \dfrac{2r_1 \cdot \cos\varphi}{v_{1,2}} \\ \Delta S_{1,2} \approx \dfrac{2r_2}{v_{1,2} \cos\varphi} \end{cases} \tag{19}$$

This enables us to find the transit impact parameter, projected to the line of sight:

$$b = r_1 \sin\varphi \approx r_1 \cdot \sqrt{1 - \frac{r_2}{r_1} \cdot \frac{\Delta W_{1,2}}{\Delta S_{1,2}}} \tag{20}$$

Combining this with (eq. 8) we can deduce the inclination angle

$$\sin i = \sqrt{1 - \left(\frac{b_{1,2}}{d_{1,2}}\right)^2} \approx \sqrt{1 - \left(\frac{r_1}{a}\right)^2 \cdot \left(\frac{1 \mp e\sin\omega}{1 - e^2}\right)^2 \cdot \left(1 - \frac{r_2}{r_1} \cdot \frac{\Delta W_{1,2}}{\Delta S_{1,2}}\right)} \tag{21}$$

This equation allows us to extract the inclination angle from either of the two dips in the light curve. Ideally, one should perform a weighted average of the two results, weighting the result from the deeper dip more than the shallower one, so to minimize the total error. In practice, a noisy shallow dip can give an enormous error, so it often more robust to simply ignore it altogether. In our experience this error is very small in comparison with the errors brought in by approximations listed above. In any case we must make sure the results are within the bounds defined by (eq. 1):

$$1 \geq \sin(i) > \sqrt{1 - \left(\frac{r_1 + r_2}{a}\right)^2} \tag{22}$$

When implementing this procedure, one should be well aware of the pitfalls involved in the measurements of ΔW and ΔS with smoothed data. Setting ΔW as the FWHM is a good approximation when the ingress/egress are nearly symmetric around their respective midpoints (e.g. in “flat-bottom” dips) and when the smoothing length scale (e.g. kernel size) is far smaller than the FWHM. The measurement of ΔS is very sensitive to the smoothing method used. For most simple smoothing methods the ingress/egress will be artificially widened, causing the measured value of ΔS to be substantially larger than it really is. The smoothing method employed in DEBiL is a spline fit through a moving kernel. This smoothing method is quite simple and robust, but if the kernel is larger than the ingress/egress it will broaden them. Fortunately there is an analytical correction for this effect, using a linear ingress/egress approximation [Seager 2003] for first order

smoothing (eq 23a) and second order smoothing (eq. 23b). It is convenient to scale the measurement values to units of the kernel length (H):

$$\frac{\Delta S_{corrected}}{H} = \begin{cases} \frac{\lambda}{2} + \sqrt{\lambda - 1}, & 1 \le \lambda \le 2 \\ \lambda & 2 \le \lambda \end{cases} \tag{23a}$$

$$\frac{\Delta S_{corrected}}{H} = \begin{cases} \sqrt{\frac{9}{5} - \frac{4}{5\lambda} - \frac{\lambda^2}{4}}, & c_1 \le \lambda \le c_2 \\ \frac{\lambda}{2} + \sqrt{\frac{9}{5} - \frac{2}{5} \cdot \sqrt{24 - 10\lambda}}, & c_2 \le \lambda \le 2 \\ \lambda & 2 \le \lambda \end{cases} \tag{23b}$$

Where: $\lambda \equiv \frac{\Delta S_{measured}}{H}$

Both c_1, c_2 have lengthy exact representations. They approximate to:

$c_1 \approx 0.45776745$; $c_2 \approx 0.64646183$

This result gives us the minimum expected values for $\Delta S_{measured}$, corresponding to an ingress/egress that is a perfect step function. For first order smoothing: $\Delta S_{measured} \ge H$ and for second order smoothing: $\Delta S_{measured} \ge H \cdot c_1$

DEBiL performs second order smoothing, but with a variable size kernel. The kernel grows and contracts so that it always contains a constant number of data points. Typical light curves, with the exception of those with periods very close to an integer number of days, will have their data points spread out in an approximately flat distribution. In these cases the kernel will have a nearly constant length.

2.4 Light-curve simulation

2.4.1 Calculating the projected distance

We will begin by finding the projected distance (D) between the star centers. There is a simple analytical solution for circular orbits (e=0):

$$D^2 = a^2 \cdot \left[1 - \sin^2\left(\frac{2\pi}{P}(t - t_0) + \omega\right) \cdot \sin^2 i\right] \tag{24}$$

With the degeneracy:

$$\omega - \frac{2\pi}{P} t_0 = const \tag{25}$$

The general case is more complex, requiring a numerical calculation of the eccentric anomaly (E) first:

$$\frac{2\pi}{P}(t - t_0) = E - e \cdot \sin E \tag{26}$$

Which can be solved analytically:

$$D^2 = a^2 \cdot \left[\left(1 - e \cdot \cos(E)\right)^2 - \left(\left(\cos E - e\right) \cdot \sin \omega + \sqrt{1 - e^2} \cdot \sin E \cdot \cos \omega \right)^2 \cdot \sin^2 i \right] \quad (27)$$

2.4.2 Limb darkening

Though a square-root law fits better for I-filter limb darkening [Claret 95], this requires doubling the number of computations, with a very small benefit compared to the error in the approximation of taking a solar-like limb darkening for all stars. Instead, we will use the quadratic law fit, which is almost as good.

$$I(\theta) \equiv B \cdot \left[1 - \tilde{a}(1 - \cos\theta) - \tilde{b}(1 - \cos\theta)^2\right] \quad (28)$$

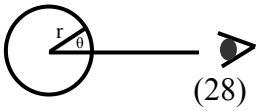

For solar-like limb darkening we use: $\tilde{a} = 0.3542$ and $\tilde{b} = 0.1939$ [Claret 2003]
From this we can construct intensity functions of the front and back stars:

$$I_{front}(r) \equiv I\left(\cos\theta = \sqrt{1 - \left(\frac{r}{r_{front}}\right)^2}\right) \quad (29a)$$

$$I_{back}(r) \equiv I\left(\cos\theta = \sqrt{1 - \left(\frac{r}{r_{back}}\right)^2}\right) \quad (29b)$$

2.4.3 Calculating observed intensity

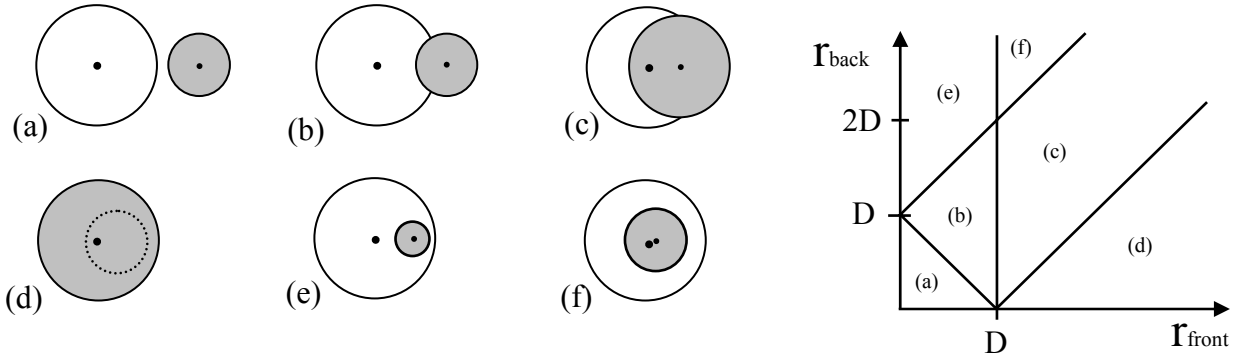

Figure 9: The left side shows the six possible cases for binary orientation. The back star is white and the front star is grey. The right diagram proves that these are indeed all the cases, by showing the appropriate classification for any positive value of back star radius and front star radius, with a given distance (D) between their centers.

Given r1, r2 and D (in arbitrary units, with a=1), one can easily find the exposed disk area seen by a given observer. Unfortunately, there is not one but six different formulae that need to be used in different cases.

The intensity of the front star: (the star doing the eclipsing)

$$I_{tot;front} = 2\pi \int_0^{r_{front}} r \cdot I_{fonrt}(r) dr \tag{30}$$

The angle of the back star's eclipsed arc:
(It is only defined when the stars' circumferences intersect)

$$\alpha(r) = 2 \cdot \arccos\left(\frac{r_{front}^2 - r^2 - D^2}{2Dr} \right) \tag{31}$$

In order to simulate the light curve of a given binary system, we must divide it into distinct segments, each of which will be solved by different equation. In total there are six types of segments (fig. 9), though any one light curve will only include part of them. The determination of which segment to use at any given time is determined by six corresponding cases of the projected orientation of the binary:

Case (a) – no intersection

$$I_{tot} = I_{tot;front} + 2\pi \int_0^{r_{back}} r \cdot I_{back}(r) dr \tag{32a}$$

Case (b) – intersection, where front is not over back's center

$$I_{tot} = I_{tot;front} + 2\pi \int_0^{D-r_{front}} r \cdot I(r) dr + \int_{D-r_{front}}^{r_{back}} r \cdot I(r) \cdot \alpha(r) dr \tag{32b}$$

Case (c) – intersection, where front is over back's center

$$I_{tot} = I_{tot;front} + \int_{r_{front}-D}^{r_{back}} r \cdot I(r) \cdot \alpha(r) dr \tag{32c}$$

Case (d) – back is completely eclipsed by front

$$I_{tot} = I_{tot;front} \tag{32d}$$

Case (e) – overlap, where front is not over back's center

$$I_{tot} = I_{tot;front} + 2\pi \int_0^{D-r_{front}} r \cdot I(r) dr + \int_{D-r_{front}}^{D+r_{front}} r \cdot I(r) \cdot \alpha(r) dr + 2\pi \int_{D+r_{front}}^{r_{back}} r \cdot I(r) dr \tag{32e}$$

Case (f) – overlap, where front is over back's center

$$I_{tot} = I_{tot;front} + \int_{r_{front}-D}^{D+r_{front}} r \cdot I(r)\alpha(r)dr + 2\pi \int_{D+r_{front}}^{r_{back}} r \cdot I(r)dr \qquad (32f)$$

Note that all but the integrals involving α(r) can be easily solved analytically.

2.5 Numerical optimization

The numerical optimization algorithm lies at the heart of the DEBiL program and typically takes the lion's share of the CPU time. The underlying procedure is quite straightforward. It begins with a guess for the eclipsing binary parameters (section 2.3), simulates their corresponding light curves (section 2.4) and compares it with the given data points to calculate the χ_ν^2 of the model with the guessed parameters. This result is then compared with previous guessed parameters and their resulting χ_ν^2 to construct another, hopefully better, parameter guess. This is repeated until the parameters converge or until a maximum number of iterations are reached. The optimization algorithm for finding subsequent guesses has the goal of locating the global minimum[4] of χ_ν^2. Like most optimization problems, this is a hard problem, especially since χ_ν^2 is a non-analytic and highly non-linear 8-dimentional function. In addition, calculating partial differentials of this function turns out to be difficult, which prevents us from using many types of optimization algorithms. The most problematic feature of the χ_ν^2 function is that it has many local minima. This means that the cruder the convergence procedure, the more likely it is that the resulting solution will only be a local minimum. In fact, the only way to guarantee finding the global minimum in χ_ν^2 is by systematically scanning all the points in the 8-space, within the resolution of the minimum's scale length. This brute force approach is clearly impractical in our case. The best-known alternative is to use a Monte Carlo approach. Today, the two most popular optimization algorithms of this kind are Genetic algorithms [Holland 1992 ; Charbonneau 1995 ; Charbonneau 2002] and the Downhill Simplex method with simulated annealing [Nelder 1965 ; Kirkpatrick 1983 ; Vanderbilt 1983 ; Otten 1989 ; Press 2002]. The fundamental difference between these two approaches is that the former requires a large number of initial guesses and combines the best *two* to create the next guess and the latter starts with a relatively small number of initial guesses (the number of dimensions plus one), and creates the next guess using a weighted linear combination of *all* of them. In both cases, a random perturbation is added to the resulting next guess (i.e. a mutation or a thermal fluctuation), which is what enables them to reach a global minimum with a substantially higher probability than "greedy" algorithms, which only consider the best result of each iteration. As stated

[4] In theory, if the data are noisy or if important physical effects are not included in the model, the true physical solution may not be exactly at the global minimum. Since there is no way of knowing this in advance, we will assume that the global minimum is the solution with the highest probability of being correct and try to solve for it.

earlier, the price for this is a significant increase in the convergence time. Determining the optimal size of the perturbations and how they should change in time is problem specific and depends on the available computational resources. In most cases, the perturbations sizes should diminish so to remain small compared to the difference between the current value and global minima. It should be noted that in some cases one should actually increase the perturbations in order to avoid stagnation in the convergence process [Charbonneau 2002].

The Downhill Simplex method with simulated annealing algorithm was selected for the DEBiL program because of its simplicity and elegance. The amplitude of the random perturbations (annealing temperature) begin large and diminish (cool down) exponentially with the number of iterations. In the current implementation of the pipeline, it runs 10,000 iterations per fit, during which time the annealing temperature falls by 15 e-folds (a factor of about three million). Since the convergence rates often intermittently slows down and speeds up, it is not advised to stop the fitting algorithm just because the convergence rate slows down somewhat.

For algorithms such as this one, were the best solution could be severely perturbed negatively, then overwritten and lost, it is often recommended to add a component to the algorithm, known as "elitism" [Aldous 1994]. In this component, the best solution is always backed up. If it is overwritten, it is reinserted after a certain number of iterations. Alternatively, the whole state machine may be reset back to a point where it gave the best result so far. Unfortunately, in practice "elitism" has a net detrimental effect since it strongly reduces the ability of the downhill simplex method to perform wide searches. In our implementation, we back up the best solution, but only employ it after the final iteration.

To improve the efficiency of the algorithm, we vary the numerical integration step size throughout the convergence process. At the beginning of the convergence, when the fit is crude and so the χ^2_ν is large, we can tolerate larger integration errors. As the χ^2_ν decreases, the integration step is made smaller so that the integration error is kept at approximately the same fraction of the fit error. Since in some cases, the integration errors may introduce non-negligible systematic errors, the last part of the convergence is run with the minimal integration step.

Finally, after the primary convergence with the downhill simplex is completed, a simple "greedy" fit is run, to guarantee that the convergence result is very close to the χ^2_ν local minimum (hopefully also the global minimum).

2.6 Post-analysis

2.6.1 The 180-degree rotation degeneracy

Up until this point we selected arbitrarily which of the stars will be index 1 and which will be index 2. In order to remove this arbitrariness, we can reset the indexes such that: $r_1 \geq r_2$. This degeneracy is equivalent to rotating the system by 180 degrees, so if we choose to swap the indexes, we need to perform the following transformations:

$$\begin{cases} r_1 \leftrightarrow r_2 \\ B_1 \leftrightarrow B_2 \\ \omega \rightarrow \omega + \pi \end{cases} \tag{33}$$

This has the effect of guaranteeing that: $r_2 \leq \frac{1}{2}$.

2.6.2 Finding the mean density:

One of the most important criteria for selecting "interesting" binaries for follow-up is its stellar density. Unfortunately, the parameters that can be extracted from the light curve fitting do not provide us with enough information for deducing the density of any one of the stars in the binary

Using Kepler's law for binary systems:

$$a^3 = G(m_1 + m_2)\left(\frac{P}{2\pi}\right)^2 \tag{34}$$

We can define a mean density using only the period (P) and semi-major axis (a), as the sum of the stars' masses divided by the sum of their volumes:

$$\overline{\rho} \equiv \frac{m_1 + m_2}{\frac{4}{3}\pi r_1^3 + \frac{4}{3}\pi r_2^3} = \frac{\frac{a^3}{G}\left(\frac{2\pi}{P}\right)^2}{\frac{4}{3}\pi\left(r_1^3 + r_2^3\right)} = \frac{3\pi}{GP^2\left(R_1^3 + R_2^3\right)} \approx \frac{0.01893\frac{g}{cm^3}}{P_{day}^2\left(R_1^3 + R_2^3\right)} \approx \frac{0.01344\rho_\Theta}{P_{day}^2\left(R_1^3 + R_2^3\right)} \tag{35}$$

Where: $R_{1,2} \equiv \frac{r_{1,2}}{a}; P_{day} \equiv \frac{P}{1day}$

It should be noted here that if the stars' have very different sizes (i.e. giant-dwarf binary), their mean density will be dominated by the larger one, since:

$$\overline{\rho} = \frac{\left(\frac{r_1}{r_2}\right)^3 \rho_1 + \rho_2}{\left(\frac{r_1}{r_2}\right)^3 + 1} \tag{36}$$

2.6.3 Finding the density upper limit:

Since this value will probably be used, primarily, as a "red flag" in data mining, it may be useful in some cases to provide an upper limit to the density of the stars.

Setting, without limiting generality, that $r_1 > r_2$:

$$\overline{\rho}_{\max} \equiv \frac{m_1 + m_2}{\frac{4}{3}\pi r_2^3} = \overline{\rho} \cdot \left(1 + \left(\frac{r_1}{r_2}\right)^3\right) = \overline{\rho} \cdot \left(1 + \left(\frac{R_1}{R_2}\right)^3\right) \approx \frac{0.01893 \frac{g}{cm^3}}{P_{day}^2 R_2^3} \approx \frac{0.01344 \rho_\Theta}{P_{day}^2 R_2^3} \tag{37}$$

2.6.4 Error estimation:

There is an inherent difficulty in measuring the error of any of the fitted parameters since it is not known whether the convergence indeed reached the global minimum or only a local minimum. As a result, a good fit with a small χ_ν^2 could still be a local minimum and far away from the global minimum. The only secure indication that the solution is accurate is if its χ_ν^2 is approximately 1, which in turn requires that the given data error be accurate. Thus, with all else being equal, we want a higher value of χ_ν^2 to prompt a larger parameter error estimated, since we are likely farther away from the global minimum or the eclipsing binary system has important physics we did not model.

The underlying idea behind estimating the errors is to see how sensitive the χ_ν^2 is to varying each one of the parameters by a small amount (ideally infinitesimal). Since the parameters are not orthogonal, once a given parameters is varied, the remaining parameters need to be refit. This is implemented by running the "greedy fit" procedure, while holding the given parameter fixed. If done properly, this has the effect of giving the result we would have got had all the parameters been orthogonal. We know that the solution is at a minimum (local or global), so the partial Taylor expansion becomes:

$$\chi_\nu^2(p_1,..,p_{i-1},p_i+\Delta p_i,p_{i+1},..,p_n) \approx \chi^2(p_1,..,p_i,..,p_n) + \frac{(\Delta p_i)^2}{2} \cdot \frac{\partial^2}{\partial p_i^2}\left(\chi_\nu^2\right) \tag{38}$$

In almost all cases the remaining terms are negligible, in which case it is indeed enough to test a single variance for each parameter. In practice we need to test both Δp_i and $(-\Delta p_i)$, since one of them could push χ_ν^2 over a discontinuity, although this is an unlikely occurrence.

The simplest definition of the error of a given parameter (p_i), which is consistent with all the above requirements, is setting it to the minimal parameter shift (Δp_i) such that after refitting, the value of χ_ν^2 doubles. By extrapolating from (eq. 38), we can define:

$$Error(p_i) \equiv \underset{\Delta p_i \to 0}{Lim}\left(\Delta p_i \cdot \sqrt{\frac{\chi_\nu^2(p_1,..,p_i,..,p_n)}{\chi_\nu^2(p_1,..,p_{i-1},p_i+\Delta p_i,p_{i+1},..,p_n) - \chi_\nu^2(p_1,..,p_i,..,p_n)}}\right) \tag{39}$$

In practice the parameter shift (Δp_i) is determined, as the smallest value for which the total numerical round-off error remains negligible.

2.7. Executing DEBiL

DEBiL was written with compatibility and ease of execution as a primary goal. The source code is a single module, entirely written in standard ANSI-C. As such, it does not require a makefile and should compile even on any operating system with an ANSI-C compiler. It has been tested on Solaris/DOS/Windows environments with a variety of compiler optimization switches. In addition, it can be compiled in a debug mode (only in DOS environment), where one can graphically monitor both the "first guess" and the convergence process.

The input required is a text file with the list of the light curve files and their respective periods. The outputs are two text files, one containing the best fit parameters for all the light curves with acceptable fits and one that contains all the warnings and errors[5] that occurred during the fitting process. Parallelizing DEBiL can be done by simply dividing the input file and having each processor work on a unique subset of the total light curve pool. Ideally, the size of the subsets should be proportional to the computing speed of the processor. Once all the processors have finished their tasks, the resulting files can be concatenated.

3. Results

Listed below are the histogram plots of the distribution of each of the eight model parameters as well as the results of a few statistical tests.

[5] Similar to compilers, we use warning messages to alert the user of suspicion situations that can be corrected or ignored and errors messages to indicate non-correctable (fatal) problems that prompt the rejection of the given light curve.

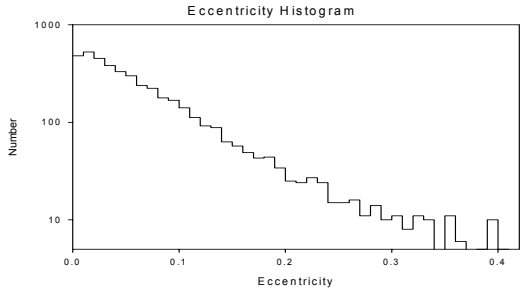

Figure 10: The distribution of eccentricities. It seems to support an exponential distribution: $p \sim \exp(-k \cdot ecc)$ **with** $k \approx 13.7 \pm 0.3$

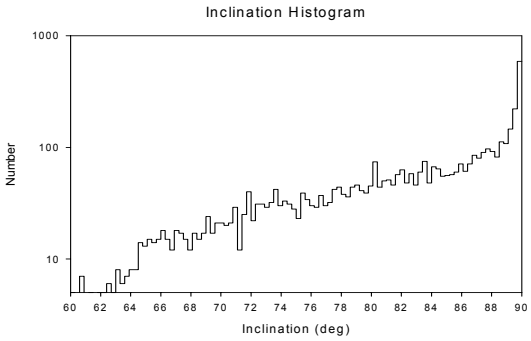

Figure 11: The distribution of inclination angles. The steep rise towards 90 degrees is due to the strong selection effect, described in eq. 1

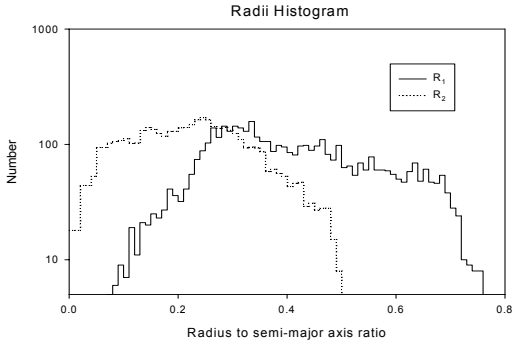

Figure 12: The distribution of radii, in units of their combined semi-major axis (a). The solid line is the radius of the larger star in the binary pair; the dashed line is for the smaller one. The cutoff at the small radii end is due to selection effect described in eq. 2

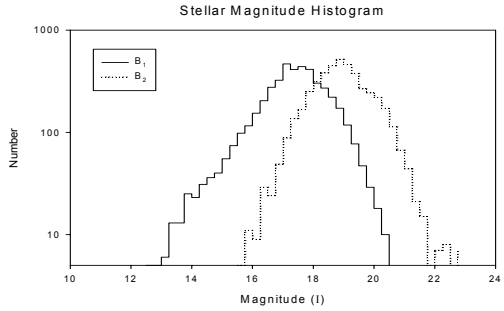

Figure 13: The distribution of I-filer magnitudes The solid line is the I-band magnitude of the larger star in the binary pair; the dashed line is for the smaller one. Both the upper and lower cutoffs are determined by the selection criteria of OGLE II

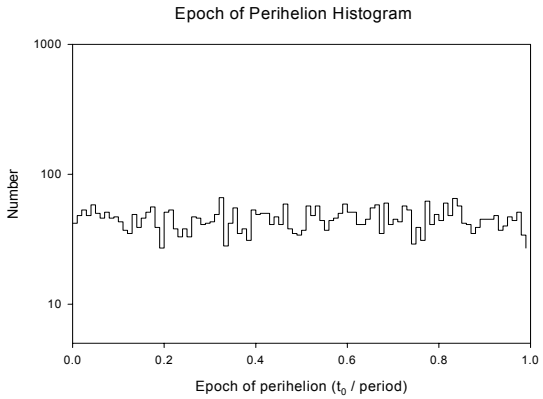

Figure 14: The distribution of epochs of perihelion, in units of the period, modulo 1. We expect no preference in epoch of perihelion. The results are consistent with a flat distribution. This plot can be seen as a sanity check for the fitting program

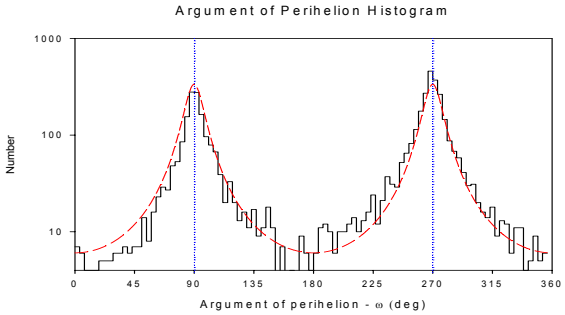

Figure 15: The distribution of the arguments of perihelion. We would expect no preference and therefore a flat distribution. In fact, we see a strong preference for 90 and 270 degrees (or π/2 and –π/2 radians, both marked by a vertical dotted line). The cause of this effect is due to the fact that $(e\cos\omega)$ is usually known quite accurately, while $(e\sin\omega)$ typically has a considerably larger error since it is deduced from the widths of the light curve dips [Etzel 1991]. The dashed curve is a best fit to a model, which assumes that both $(e\cos\omega)$ and $(e\sin\omega)$ have Gaussian distributions around zero. The only parameter in the model that is varied is the ratios of the standard deviations of the two distributions. The best fit is achieved when the standard deviation of the former is 7.471 times smaller than the standard deviation of the latter.

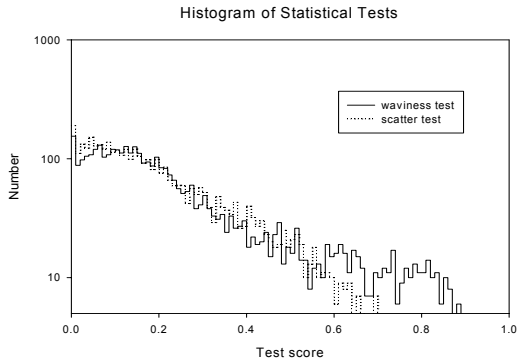

Figure 16: The distribution of two statistical tests- waviness test and scatter test. These tests, which are described in appendix B, are indicators for how good the model fit is. The lower the tests score the better the fit.

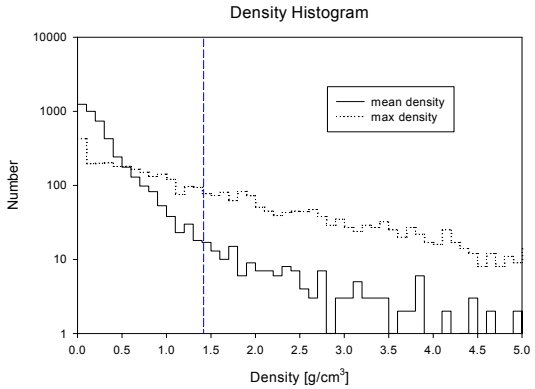

Figure 17: The distribution of the mean density and max density approximations (see subsections 2.6.2 and 2.6.3). The vertical dashed line indicates the mean solar density. The conclusion from this distribution is that most of the stars seen are massive main sequence stars or giants (only the longer period binaries).

4. Conclusions

In this paper we presented a new method for rapidly fitting a large number of light curves to simple eclipsing binary models. Although the models presented do not include many of the complexities considered by other more complete models (e.g. spots, flares, tidal interaction, gravity darkening, reflections, 3rd star blending, etc.), it is a good theoretical fit for detached binaries, where these effects are negligible. Unfortunately, in light curve surveys, there is a strong preferential bias towards observing interacting and semi-detached systems. This is both because of the geometric requirement of seeing eclipses (eq. 1) and because detached systems will generally have longer periods, often well beyond the span of the observations. In our case, the cutoff was set at 200 days, which corresponds to orbital radii typically under 1AU. As more light curves are collected, for longer durations, there will be a growing need to analyze them automatically. DEBiL will enable finding specific interesting cases in real time, as well as to relieving the need for manual model fitting to an overwhelming quantity of data.

Appendix A. – A useful approximation:

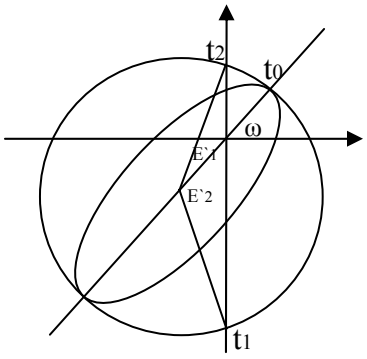

Figure 18: This diagram is similar to figure 7, but with an approximation to mean anomalies.

Here we will discuss a somewhat more appealing method for finding the system's eccentricity and argument of perihelion, for nearly circular orbits. We will use a quantity similar to the mean anomaly (see fig. 18). This quantity converges with the mean anomaly for small eccentricities (e) or small arguments of perihelion (ω). This quantity has useful geometric properties that greatly simplify the results.

We will begin by defining:

$$\xi \equiv \arccos(e\cos\omega) \tag{A1}$$

In addition, from fig. 18

$$\cos(E_{1,2}+\omega) \approx e\cos\omega \Rightarrow E_{1,2} \approx -\omega \mp \xi \tag{A2}$$

Setting this into:

$$\frac{2\pi}{P}\left((t_2-t_0)-(t_1-t_0)\right) = (E_2-E_1) - e(\sin E_2 - \sin E_1) \tag{A3}$$

$$\frac{2\pi}{P}(t_2-t_1) = 2\xi - \sin 2\xi \tag{A4}$$

This equation can be conveniently solved using the same method used to solve for the mean anomaly in Kepler's equation (eq.14). Finally, by converting from Cartesian to polar coordinates, we can easily deduce the values for the eccentricity (e) and the argument of perihelion (ω):

$$\begin{cases} e\cos\omega = \cos\xi \\ e\sin\omega = \dfrac{W_1 - W_2}{W_1 + W_2} \end{cases} \tag{A5}$$

Finally, by summing the mean anomalies, we can retrieve the epoch of perihelion (t_0). As expected, to first order when $\omega = 0$, the epoch of perihelion is midway between the two dips. When $\omega \neq 0$, t_0 is offset proportionally according to (eq. 25). Now we see that there is in fact an additional component that can grow to be as large as: $\frac{1}{4\pi} \approx 0.08$

$$\frac{2\pi}{P}\left(\left(t_1 - t_0\right) + \left(t_2 - t_0\right)\right) = \left(E_1 + E_2\right) - e\left(\sin E_1 + \sin E_2\right) \tag{A6}$$

When setting (eq. A2)

$$t_0 = \frac{t_1 + t_2}{2} + \frac{P}{2\pi}\left(\omega - e\sin\omega\cos\xi\right) = \frac{t_1 + t_2}{2} + \frac{P}{4\pi}\left(2\omega - e^2\sin\left(2\omega\right)\right) \tag{A7}$$

Appendix B. - Statistical tests:

Scatter score-

This test quantifies the systematic scatter of data above or below the model. It is essentially a normalized correlation function between neighboring residuals. If we sort the n data points and corresponding n model points by phase (i.e. time modulo the period), we can define:

$$\Delta X_i \equiv X_i(\text{data}) - X_i(\text{model}) \tag{B1}$$

$$ScatterScore \equiv \frac{\Delta X_n \cdot \Delta X_1 + \sum_{i=2}^{n} \Delta X_{i-1} \cdot \Delta X_i}{\sum_{i=1}^{n} \Delta X_i^2} = \frac{\left\langle \Delta X_{i-1} \cdot \Delta X_i \right\rangle}{\left\langle \Delta X_i^2 \right\rangle} \tag{B2}$$

The Cauchy-Schwartz inequality guarantees that the scatter score will always be between one and minus one. A score of one represent a case where all the data is either entirely above or entirely below the model. A score of zero represents an ideal case where the data is distributed randomly around the model. A negative score, though possible, are generally considered unphysical (e.g. if even data points are above the model and the odd data point are below). The purpose of this test is to quantify the quality of the model fit independently of the χ_ν^2 test. While the χ_ν^2 test considers the amplitude of the residuals, the scatter score considers their distribution.

Waviness-

This is a special case of the scatter score. Here we look only at the data points in the light curve's plateau (i.e. the region in the phased curve between the eclipsing dips, where both stars are fully exposed). The Waviness score is the scatter score of these points around their median. The purpose of this test is to get a model independent measure of where a given eclipsing binary system falls on the continuum ranging from fully detached, through semi-detached until interacting binaries.

Chi score-

One of the problems with using reduces chi square (χ_ν^2) is that the error estimates may be too large, causing the reduced chi square to be too small. One of the easiest ways to handle this problem is by comparing best-fit model reduced chi square with a bogus

model reduced chi square. Two useful such bogus models are a constant (in our case set to the average amplitude of the data) and a spline (in our case a second order spline of the phased light curve). The former is expected to have a larger reduced chi square than the best-fit model, while the latter is expected to have a smaller reduced chi square. We define the chi score to be a normalization of the best-fit model reduced chi square, such that if it equals the constant's reduced chi square the score will be 0 and if it equals the spline's reduced chi square the score will be 1.

$$ChiScore \equiv \frac{\chi_\nu^2(const) - \chi_\nu^2(\mathrm{mod}\,el)}{\chi_\nu^2(const) - \chi_\nu^2(spline)} \tag{B3}$$

If the error estimate is too small or too large, it will affect all the reduced chi square values proportionally and will be canceled out. As stated previously, the chi score is typically between 0 and 1, though exceptionally good fits may have a chi score above 1. Since the binary model has full control over the DC component, a best-fit model should never have a negative chi score.

Appendix C. – examples of DEBiL fits:

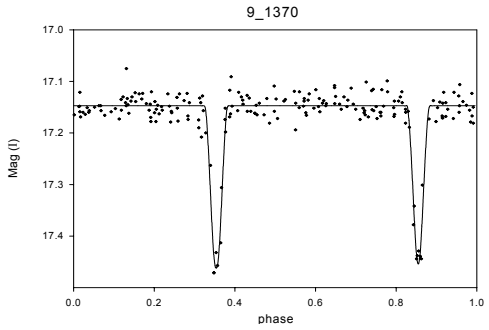

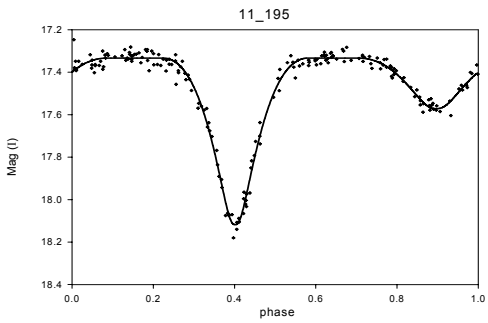

Filename	bul_sc9_1370.dat	bul_sc11_195.dat
Period (days)	4.867560	0.794272
Eccentricity	0.008200	0.043023
R1	0.117943	0.511921
R2	0.066616	0.395430
B1	17.468384	17.572022
B2	18.625728	19.098312
Sin(i)	0.998392	0.992910
Epoch of perihelion	0.886450	0.428112
Argument of perihelion (ω)	1.771178	1.752350
χ_ν^2	0.990924	1.272669
Waviness score	-0.088936	0.316888
Scatter score	-0.109735	0.098618
Mean density [g/cm³]	0.412628	0.153104
Max density [g/cm³]	2.702633	0.485292

References:

Alard, C. and Guibert, J., The DUO single lens candidates. I. The 1994 campaign, Astronomy and Astrophysics, vol. 326, p. 1-12 (1997)

Alcock, C. et al., The RR Lyrae Population of the Galactic Bulge from the MACHO Database: Mean Colors and Magnitudes, Astrophysical Journal vol.492, p. 190 (1998)

Aldous D. and Vazirani U., "Go With the Winners" Algorithm, Proc. of FOCS, p. 492-501 (1994)

Allen C.W., Astrophysical Quantities, Springer Verlag, 4th edition (2000)

Beaulieu, J. P. et al., Spectroscopic studies of the two EROS candidate microlensed stars, Astronomy and Astrophysics, vol. 299, p. 168 (1995)

Charbonneau P., Genetic Algorithms in Astronomy and Astrophysics, The Astrophysical Journal Supplement Series, vol. 101, p. 309-334 (1995)

Charbonneau P., An introduction for Numerical Optimization, NCAR Technical Notes, 450+IA (2002)

Claret, A. et al., Linear and non-linear limb-darkening coefficients for the photometric bands R I J H K, Astronomy and Astrophysics Supplement, vol.114, p.247 (1995)

Claret, A., Very low mass stars: non-linearity of the limb-darkening laws, Astronomy and Astrophysics, vol. 335, p. 647-653 (1998a)

Claret, A., Comprehensive tables for the interpretation and modeling of the light curves of eclipsing binaries, Astronomy and Astrophysics Supplement, vol.131, p.395-400 (1998b)

Crotts, A., M31 - A unique laboratory for gravitational microlensing, Astrophysical Journal, Part 2 - Letters, vol. 399, no. 1, p. L43-L46 (1992)

Danby, J.M.A., Fundamentals of Celestial Mechanics, Macmillan (1964)

Etzel, P. B., A Simple Synthesis Method for Solving the Elements of Well-Detached Eclipsing Systems, Photometric & Spectroscopic Binary Syst. NATO1981 p.111 (1981)

Etzel, P. B., Detached Binaries and Simple Computer Codes for Fewer Rocky Roads, International Amateur-Professional Photoelectric Photometry Communication, no. 45, p.25 (1991)

Genet R., Hayes D., “Robotic Observatories: A Handbook of remote-access personal-computer astronomy”, Autoscope Corp. (1989)

Hall, D.S., Variable Stars in the Hertzprung-Russell Diagram, Robotic Telescopes. Current Capabilities, Present Developments, and Future Prospects for Automated Astronomy, ASP Conference Series, vol. 79 (1995)

Holland, J.H., Adaptation in Natural and Artificial Systems. Second edition. Cambridge: MIT Press (1992)

Kaluzny, J. et al., DIRECT Distances to Nearby Galaxies Using Detached Eclipsing Binaries and Cepheids. I. Variables in the Field M31B, astro-ph/9703124

Kirkpatrick, S., Gelatt, C.D. and Vecchi, M.P., Science, vol. 220, p. 671-680 (1983)

Mizerski, T. and Bejger, M., Automatic Variability Analysis of Bulge Stars in OGLE-II Image Subtraction Database, Acta Astronomica, vol. 52, p. 61-80 (2002)

Nelder, J. A. and Mead, R., A Simplex Method for Function Minimization, Computer Journal, vol. 7, p. 308-313 (1965)

Nelson, B. and Davis, W. D., Eclipsing-Binary Solutions by Sequential Optimization of the Parameters, Astrophysical Journal, vol. 174, p. 617 (1972)
Otten, R.H.J.M. and van Ginneken, L.P.P.P., The Annealing Algorithm, Kluwer Academic Publishers (1989)
Paczynski, B., Gravitational microlensing by the galactic halo, Astrophysical Journal, part 1, vol. 304, p. 1-5 (1986)
Paczynski, B., Detached eclipsing binaries as primary distance and age indicators, Conference Paper, Space Telescope Science Institute Series, The Extragalactic Distance Scale, edited by M. Livio (Cambridge University Press), p. 273-280. (1997)
Phillips, A. C. and Davis, L. E., Astronomical Data Analysis Software and Systems IV, ASP Conf. Ser. 77, p. 297 (1995)
Press, W. H. et al., Numerical Recipes in C++, Cambridge University Press (2002)
Rencher A. C., Methods of Multivariate Analysis, Wiley-Interscience (2002)
Schwarzenberg-Czerny, A., On the advantage of using analysis of variance for period search, Mot. Not. R astr. Soc., vol. 241, p. 153-165 (1989)
Schwarzenberg-Czerny, A., Fast and Statistically Optimal Period Search in Uneven Sampled Observations, Astrophysical Journal Letters vol. 460, p. L107, (1996)
Seager, S. and Mallén-Ornelas, G., Extrasolar Planet Transit Light Curves and a Method to Select the Best Planet Candidates for Mass Follow-up, American Astronomical Society, 201st AAS Meeting, #21.05; Bulletin of the American Astronomical Society, vol. 34, p. 1138 (2002)
Seager, S. and Mallén-Ornelas, G., A Unique Solution of Planet and Star Parameters from an Extrasolar Planet Transit Light Curve, The Astrophysical Journal, vol. 585, issue 2, p. 1038-1055 (2003)
Sterken, C. and Jaschek, C., Light Curves of Variable Stars: a pictorial atlas, Cambridge Press (1996)
Szalay, A. and Gray, J., The World-Wide Telescope, Science, vol. 293, issue 5537, p. 2037-2040 (2001)
Udalski, A et al., The Optical Gravitational Lensing Experiment. The Optical Depth to Gravitational Microlensing in the Direction of the Galactic Bulge, Acta Astronomica, vol. 44, p. 165-189, (1994).
Udalski A., Kubiak M., Szymanski M., Optical Gravitational Lensing Experiment. OGLE-2 - the Second Phase of the OGLE Project, ACTA Astronomica, vol. 47, p. 319-344 (1997)
Vanderbilt, D. and Louie S.G., Journal of Computational Physics, vol. 56, p. 259-271 (1983)
Wilson R. E., Devinney E. J., Realization of Accurate Close-Binary Light Curves: Application to MR Cygni, Astrophysical Journal, vol. 166, p.605 (1971)
Wilson R. E., Eccentric orbit generalization and simultaneous solution of binary star light and velocity curves, Astrophysical Journal, part 1, vol. 234, p. 1054-1066 (1979)
Wozniak, P. R. et al., Difference Image Analysis of the OGLE-II Bulge Data. III. Catalog of 200000 Candidate Variable Stars, Acta Astronomica, vol.52, p.129-142, (2002)
Wyithe, J. S. B. and Wilson, R. E., Photometric Solutions for Detached Eclipsing Binaries: Selection of Ideal Distance Indicators in the Small Magellanic Cloud, The Astrophysical Journal, vol. 559, issue 1, p. 260-274 (2001)

Lacy, C. H. S., et al., Absolute Properties of the Main-Sequence Eclipsing Binary Star BP Vulpeculae, The Astronomical Journal, vol. 126, issue 4, p. 1905-1915 (2003)
Lacy, C. H. S., et al., Absolute Properties of the Main-Sequence Eclipsing Binary Star WW Camelopardalis, The Astronomical Journal, vol. 123, issue 2, p. 1013-1022 (2002)
Lacy, C. H. S., et al., Absolute Properties of the Eclipsing Binary Star FS Monocerotis, The Astronomical Journal, vol. 119, issue 3, p. 1389-1397 (2000)
Sabby, J. A. and Lacy, C. H. S., Absolute Properties of the Eclipsing Binary Star RT Coronae Borealis, The Astronomical Journal, vol. 125, issue 3, p. 1448-1457 (2003)
Mazeh, T. at al., The Mass Ratio Distribution in Main-Sequence Spectroscopic Binaries Measured by Infrared Spectroscopy, The Astrophysical Journal, vol. 599, issue 2, p. 1344-1356 (2003)
Duquennoy, A. and Mayor, M., Multiplicity among solar-type stars in the solar neighbourhood. II - Distribution of the orbital elements in an unbiased sample, Astronomy and Astrophysics, vol. 248, no. 2, p. 485-524 (1991)